

## Attosecond electron thermalization in laser-induced nonsequential multiple ionization: hard versus glancing collisions

To cite this article: X Liu *et al* 2008 *New J. Phys.* **10** 025010

View the [article online](#) for updates and enhancements.

### Related content

- [Attosecond electron thermalization by laser-driven electron recollision in atoms](#)
- [Wavelength dependence of sub-laser-cycle few-electron dynamics in strong-field multiple ionization](#)
- [Nonsequential double ionization with polarization-gated pulses](#)

### Recent citations

- [Steering electron correlation time by elliptically polarized femtosecond laser pulses](#)  
Huipeng Kang *et al*
- [A practical theoretical formalism for atomic multielectron processes: direct multiple ionization by a single auger decay or by impact of a single electron or photon](#)  
Pengfei Liu *et al*
- [Coulomb-potential effects in nonsequential double ionization under elliptical polarization](#)  
MingYan Wu *et al*

## Attosecond electron thermalization in laser-induced nonsequential multiple ionization: hard versus glancing collisions

X Liu<sup>1</sup>, C Figueira de Morisson Faria<sup>2</sup> and W Becker<sup>3,4</sup>

<sup>1</sup> State Key Laboratory of Magnetic Resonance and Atomic and Molecular Physics, Wuhan Institute of Physics and Mathematics, Chinese Academy of Sciences, Wuhan 430071, People's Republic of China

<sup>2</sup> Department of Physics and Astronomy, University College London, Gower Street, London WC1E 6BT, UK

<sup>3</sup> Max-Born-Institut, Max-Born-Str. 2A, 12489 Berlin, Germany  
E-mail: [wbecker@mbi-berlin.de](mailto:wbecker@mbi-berlin.de)

*New Journal of Physics* **10** (2008) 025010 (18pp)

Received 2 October 2007

Published 29 February 2008

Online at <http://www.njp.org/>

doi:10.1088/1367-2630/10/2/025010

**Abstract.** A recollision-based largely classical statistical model of laser-induced nonsequential multiple ( $N$ -fold) ionization of atoms is further explored. Upon its return to the ionic core, the first-ionized electron interacts with the other  $N - 1$  bound electrons either through a contact or a Coulomb interaction. The returning electron may leave either immediately after this interaction or join the other electrons to form a thermalized complex which leaves the ion after the delay  $\Delta t$ , which is the sum of a thermalization time and a possible additional dwell time. Good agreement with the available triple and quadruple ionization data in neon and argon is obtained with the contact scenario and delays of  $\Delta t = 0.17 T$  and  $0.265 T$ , respectively, with  $T$  the laser period.

<sup>4</sup> Author to whom any correspondence should be addressed.

**Contents**

<b>1. Introduction</b>	<b>2</b>
<b>2. Thermalization model</b>	<b>4</b>
<b>3. Ion-momentum distributions</b>	<b>8</b>
<b>4. Conclusions</b>	<b>13</b>
<b>Acknowledgments</b>	<b>15</b>
<b>Appendix. Evaluation of the Coulomb-scenario ion-momentum distribution</b>	<b>15</b>
<b>References</b>	<b>17</b>

**1. Introduction**

In recent years, the production of ultrashort laser pulses with intensities higher than  $10^{14} \text{ W cm}^{-2}$  has become routine. Atoms exposed to such laser pulses exhibit a number of striking phenomena. Among them, nonsequential multiple ionization (NSMI) is of fundamental interest due to the highly correlated behaviour of the participating electrons. The first signature of this phenomenon was found in the early 1980s [1], in the unexpectedly large double and multiple ionization yield (see for example, [2]). This yield may exceed the prediction of single-active-electron (SAE) models by many orders of magnitude. More recently, differential measurements of the electron-momentum distributions have confirmed that NSMI is predominantly caused in the recollision of a first-ionized electron with its parent ion (see, e.g., [3] and references therein). This is the same mechanism that is responsible for high-order harmonic generation (HHG) and high-order above-threshold ionization (HATI): an electron is freed by quasi-static tunnelling ionization at a time  $t'$ , and is driven back by the laser electric field to its parent ion, where it can rescatter, recombine or dislodge other electrons at a later time  $t$  [4].

Recollision is at the very basis of the emerging field of attosecond science [5]. The production of attosecond XUV photon pulses obviously is one of the most important consequences of this scenario. In addition, any laser-induced excitation dynamics as a consequence of this recollision scenario may be explored with attosecond time resolution. The fact that the recolliding electron is well synchronized with respect to the laser field facilitates this type of study. Indeed, the recolliding electron burst has been employed as a probe of the molecular dynamics with subangstrom spatial and subfemtosecond temporal resolution [6]. Another example would be attosecond time-resolved NSMI dynamics within atoms, for which the attosecond timescale arises naturally at the two stages of the process: Firstly, the tunnelling of the first electron is most probable during a small fraction of the laser period  $T$  ( $T \approx 2.7 \text{ fs}$  for the commonly used titanium-sapphire laser) around the field maximum. Secondly, the most important electron trajectories, which yield subsequent collision-induced NSMI processes, further confine the time range of the dynamics.

For NSMI, however, the complex dynamics involved pose a great challenge to any theoretical treatment. The inclusion of the time-dependent electron–electron interaction in a fully quantum-mechanical treatment has not yet been entirely accomplished even for the very simplest case of nonsequential double ionization (NSDI) of helium [7]. Indeed, only very recently has the time-dependent Schrödinger equation been solved in this case within a realistic three-dimensional (3D) framework and for the parameter range of interest [8]. In such studies, however, the motion of the centre-of-mass of the system is still confined to 1D. Hence,

any quantum-mechanical description of NSMI that includes the electron–electron interactions between more than one pair of electrons is probably a hopeless task in the foreseeable future.

In order to tackle such a problem and to elucidate the NSMI physics, we have recently proposed a statistical model based on the recollision scenario [9, 10]. We assumed that the first electron, freed by tunnelling ionization, driven back by the laser electric field and recolliding with its parent ion, shares its kinetic energy with  $N - 1$  bound electrons. All  $N$  electrons are then freed after a time delay  $\Delta t$  subsequent to the recollision time  $t$ . This time delay gives an upper limit for a ‘thermalization time’, which is necessary for the kinetic energy to be redistributed among the  $N$  electrons. Similar statistical models have been widely employed in many areas of physics; including atomic, molecular, nuclear and particle physics [11]–[13]. By comparing the measured momentum distributions of multiply charged neon ions to those predicted by our thermalization model, we were able to infer a thermalization time of less than 500 attoseconds [9] and thus, to our knowledge, to unveil the thermodynamics within a single atom for the first time (to the extent one can speak of thermodynamics for the case of 3 or 4 electrons). We have further investigated the influence of the thermalization time on two types of collisions, i.e. the ‘slow-down’ and ‘speed-up’ collisions [14], in the context of NSMI. We found that these two types of collisions behave in distinct ways and lead to different distribution widths and peak momenta [10]. The peaks and widths of the overall ion-momentum distributions, when both types of collisions are present, result from the interplay between both contributions.

However, the above-mentioned statistical model on the basis of the recollision scenario has raised questions that are still waiting for an answer. For instance, the form of the electron–ion interaction, by which the returning electron transfers part of its kinetic energy to the other  $N - 1$  electrons, has been debated. In our previous papers [9, 10], we assumed a zero-range contact potential to account for this interaction, and this led to reasonably good agreement with the experimental data for neon. Such an interaction yields isotropic ( $s$ -wave) scattering only. It appears justified when the energy of the returning electron is sufficiently low so that its de Broglie wavelength is at least comparable with if not larger than the atomic diameter. In this case, the electron will not be sensitive to details of the potential so that a zero-range potential may be good enough. For higher energies, however, a Coulomb interaction between the returning electron and some ensemble of electrons that are still bound to the ion appears more natural. This would also allow for glancing collisions, where the returning electron essentially continues on its path and imparts only some fraction of its energy to the bound electrons. Only the  $N - 1$  bound electrons would then thermalize and leave at a subsequent time  $t + \Delta t$ . It is thus of interest to explore the consequences of these two different physical mechanisms in NSMI, and to find clear signatures of the very interaction that is instrumental for the thermalization and subsequent ejection of the bound electrons.

Another open question concerns the distinctly different behaviour of NSMI for different atomic targets. Recently, the final-momentum distributions of NSMI ions for both neon and argon have been measured with cold target recoil ion momentum spectroscopy (COLTRIMS) and found to be significantly different [15, 16]. The momentum distribution of multiply charged neon ions exhibits a double-hump structure with a valley at zero momentum, while the distribution of argon shows a broad peak centred at zero momentum. This behaviour is similar to what was observed earlier for NSDI of neon [17] and argon [18]. For NSDI, the difference was attributed to the contribution of an additional channel in the case of argon—the recollision-induced excitation-tunnelling mechanism, in which the second electron is excited to an intermediate excited state

by the recollision and thereafter becomes free via tunnelling [19]. This was confirmed by the observation that the contribution of this channel becomes quenched for very short laser pulses [15].

On the other hand, it has been found that the peaks and widths of the momentum distributions very strongly depend on the thermalization time within the thermalization model [9]. With sufficiently large thermalization times, the computed ion-momentum distributions start to concentrate near zero momentum and resemble those obtained with excitation-tunnelling. Thus, a large thermalization time might provide an alternative way of looking at momentum distributions localized in this region, at least in the case that more than two electrons are involved. In this context, one should keep in mind that in the thermalization model the specific dynamics of the system are stripped from the model, after recollision has taken place. They are only manifest in the specific value of the thermalization time, but the same value may originate from different dynamics.

In this contribution, we address the above issues. We investigate the effect of different thermalization scenarios on the ion-momentum distributions. Specifically, we focus on the interaction by which the first (recolliding) electron interacts with its parent ion. We will consider two extreme limits, namely, the infinite-range Coulomb potential and a zero-range contact potential. For the Coulomb potential, we assume that the  $N - 1$  up to the recollision still bound electrons thermalize. Physically, this means that the returning electron predominantly experiences a soft collision upon return, and continues along its path without further interaction with the ion core. Thus, only the  $N - 1$  bound electrons thermalize. For the contact potential, we consider both situations, i.e. either all  $N$  electrons thermalize and leave at the same later time  $t + \Delta t$ , or the first electron leaves immediately and only the  $N - 1$  bound electrons thermalize and are released after a time delay. Even though the former scenario would be intuitively more appropriate for the case of a collision mediated by a short-range potential, the latter allows for a more direct comparison with the soft-collision mechanism. Recent measurements of the electron–electron momentum correlation in NSDI ( $N = 2$ ) of helium exhibited features that were attributed to either ‘binary’ or ‘recoil’ collisions [20], which, respectively, closely correspond to our Coulomb or contact-potential-mediated scenarios for the case  $N = 2$ .

The paper is organized as follows. In the subsequent section, we will discuss our thermalization model, and provide explicit expressions for the ion-momentum distribution under the different types of electron–ion interaction. We will mainly focus on the Coulomb-interaction (glancing or soft collision) case, which is the new aspect brought into this paper, but we will also briefly recall the contact-interaction (hard-collision) model employed in [9, 10]. Subsequently, in section 3, we will present ion-momentum distributions computed for both scenarios and compare them with the data for Ne and Ar. For Ar, we consider only the hard-collision mechanism. The choice of a thermalization time larger than for neon yields very good agreement with the data. Finally, in section 4, our conclusions are stated. Atomic units are used throughout unless otherwise stated.

## 2. Thermalization model

We will consider models where the  $N$ -electron momentum distribution is given by

$$F(\mathbf{p}_1, \mathbf{p}_2, \dots, \mathbf{p}_N) = \int dt' R(t') \delta \left( E_0^{(N)} + E_{\text{kin}}^{(N)} - E_{\text{ret}}(t) \right) |V_{\mathbf{p}_1, \mathbf{k}}|^2. \quad (1)$$

This distribution describes a recollision scenario where the first electron (electron #1) tunnels out at the time  $t'$  at the rate  $R(t')$  for which we take the standard quasistatic tunnelling rate [21]. Thereafter, an entirely classical description is adopted. Depending on the value  $t'$  of this tunnelling time, the electron may be driven back to its parent ion by the laser electric field at the later time  $t$ , which is a function  $t(t')$  of the former and can be easily calculated from the simple-man model [4]. The electron returns to its parent ion with the velocity  $\mathbf{k} + \mathbf{A}(t)$  and the kinetic energy  $E_{\text{ret}}(t) = (1/2)[\mathbf{k} + \mathbf{A}(t)]^2$ , where  $\mathbf{k} \equiv k\mathbf{e}$  denotes its drift momentum and  $\mathbf{e}$  is a unit vector in the direction of the linearly polarized laser field. In the recollision, the electron changes its velocity from  $\mathbf{k} + \mathbf{A}(t)$  to  $\mathbf{p}_1 + \mathbf{A}(t)$  (equivalently, its drift momentum changes from  $\mathbf{k}$  to  $\mathbf{p}_1$ , which is the momentum recorded at the detector outside the field). The details of the distribution (1) now depend on the form factor  $V_{\mathbf{p}_1\mathbf{k}}$ , which is the Fourier transform of the electron–ion interaction potential, and on the relation between the available energy  $E_{\text{ret}}(t) - E_0^{(N)}$  and the kinetic energy  $E_{\text{kin}}^{(N)}$  of the  $N$  final electrons. Here,  $E_0^{(N)} = \sum_{n=2}^N I_p^{(n)}$  denotes the total ionization potential of the (up to the time  $t$  still bound)  $N - 1$  electrons with  $I_p^{(n)}$  denoting the ionization potential of the  $n$ th electron.

We will investigate two models: in the first, we take

$$V_{\mathbf{p}_1\mathbf{k}} = \text{constant}, \quad (2)$$

$$E_{\text{kin}}^{(N)} = \frac{1}{2} \sum_{n=1}^N [\mathbf{p}_n + \mathbf{A}(t + \Delta t)]^2. \quad (3)$$

According to this ansatz, the energy that is left after the up to the time  $t$  bound electrons ( $n = 2, \dots, N$ ) have been promoted into the continuum is distributed over all electrons without any dynamical bias, just according to the accessible phase space volume. In other words, the ensemble of electrons ( $n = 1, 2, \dots, N$ ) is thermalized. It is assumed that this thermalization process takes the time  $\Delta t$  to be completed. This ‘thermalization time’ parametrizes the intricate dynamics by which the returning electron shares its energy with the bound electrons. It appears natural to assume that this energy sharing will require some time. In view of the uncertainty relation, this will take place on a subfemtosecond timescale. This situation will certainly be realized for comparatively low energy of the returning electron, such that its de Broglie wavelength (after freeing the bound electrons) is comparable with or larger than the atomic diameter. However, depending on the actual dynamics, it may also yield a fair description for higher energies if the dynamics are such that  $s$ -wave scattering is dominant. Intuitively, this model describes a ‘hard’ collision since the first electron backscatters and forwardscatters with the same probability. In this scenario, the first electron in the recollision loses all memory of its distinguished role in the dynamics and is henceforth treated on the same footing as the other electrons. Below, we will refer to this model as the ‘contact scenario’. This model is an extension to NSMI of the classical model introduced for NSDI [22, 23] for  $\Delta t = 0$ .

We specify the second model by

$$V_{\mathbf{p}_1\mathbf{k}} = \frac{1}{(\mathbf{p}_1 - \mathbf{k})^2} = \frac{1}{\mathbf{p}_{1\perp}^2 + (p_{1\parallel} - k)^2}, \quad (4)$$

$$E_{\text{kin}}^{(N)} = \frac{1}{2} [\mathbf{p}_1 + \mathbf{A}(t)]^2 + \frac{1}{2} \sum_{n=2}^N [\mathbf{p}_n + \mathbf{A}(t + \Delta t)]^2. \quad (5)$$

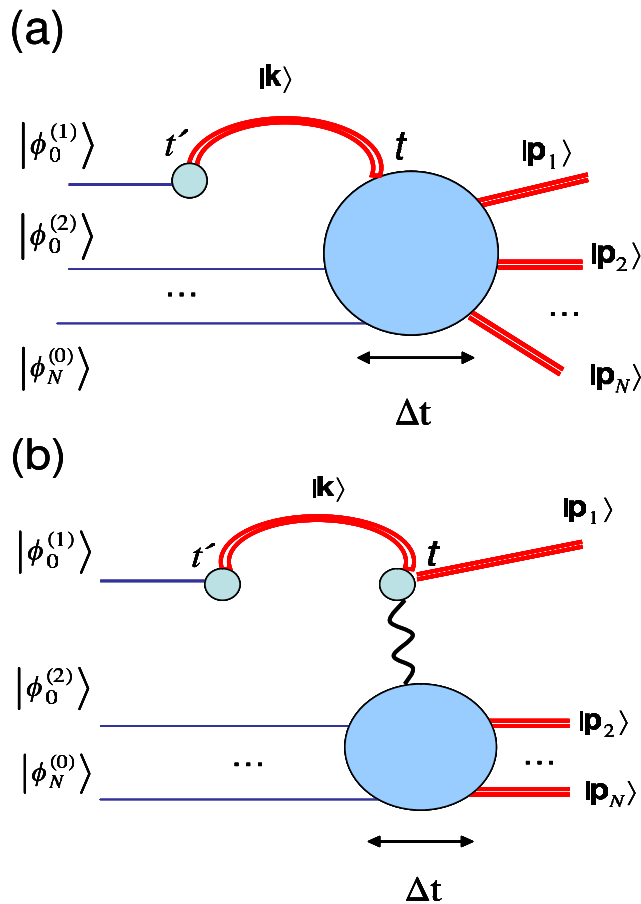


**Figure 1.** Feynman diagrams for the two models discussed in the text. (a) Thermalization of all participating electrons such that the returning electron interacts with the bound electrons in the presence of the ion via a contact interaction. (b) The returning electron gives some fraction of its energy to the bound electrons in a glancing collision mediated by the Coulomb interaction. The bound electrons subsequently thermalize in the presence of the ion. The big blob represents the dynamical process that causes thermalization, which is assumed to occur within the time interval  $\Delta t$ . Double lines represent Volkov propagators and wave functions.

Here, the returning electron undergoes a Coulomb interaction with the remaining electrons and the ion, which is reflected in the Coulomb form factor (4). The returning electron immediately leaves at the recollision time  $t$ , in contrast to the remaining electrons, which subsequently share the energy  $E_{\text{ret}}(t) - E_0^{(N)} - (1/2)[\mathbf{p}_1 + \mathbf{A}(t)]^2$  and thermalize among themselves to become free at the later time  $t + \Delta t$ . Owing to the long range of the Coulomb interaction, in this model electrons also contribute to NSMI that return at nonzero impact parameters undergoing glancing collisions. One might expect this model to be more realistic for high energies of the returning electron, corresponding to high laser intensities and comparatively low ionization potentials. We will refer to it below as the ‘Coulomb scenario’.

The first model characterized by (2) and (3) has been extensively discussed and compared with the available data in [9, 10]. Figure 1 presents the Feynman diagrams that underlie the two models. Let us discuss which one of the two may be closer to reality. The wave packet of an electron freed by tunnelling ionization has the transverse momentum spread ( $1/e$  width of the distribution of  $\mathbf{p}_\perp^2$ )  $\Delta p_\perp^2 = \omega/\gamma$ , where  $\omega = 2\pi/T$  denotes the laser frequency,

$$\gamma = \sqrt{I_p^{(1)}/(2U_p)}$$

the Keldysh parameter,  $I_p^{(1)}$  the first ionization potential of the atom, and  $U_p$  the ponderomotive energy [24]–[26]. The electron returns to the ion approximately after the time  $3T/4$ . Hence, the transverse width of the returning wave packet is

$$\Delta\rho \equiv \Delta p_\perp(3T/4) = \frac{3\pi}{2\sqrt{\omega\gamma}} \gg 1. \quad (6)$$

For all NSMI experiments in the optical or infrared regime, this is much larger than the ionic radius ( $\approx 1$  in atomic units), because  $\omega \ll 1$  in atomic units while the (dimensionless) Keldysh parameter is of the order of unity. This seems strongly to underline the significance of glancing collisions since most of the returning electrons, in terms of their classical impact parameter, miss the ion and can only interact with it via the long-range Coulomb interaction. On the other hand, the de Broglie wavelength of the returning electron is approximately

$$\lambda_{\text{dB}} = \frac{2\pi\gamma}{\sqrt{3I_p^{(1)}}} > 1, \quad (7)$$

where we used the fact that the kinetic energy of the returning electron is of the order of  $3U_p$ . This is smaller than the width  $\Delta\rho$ , but still larger than unity except when the Keldysh parameter has an unusually small value. This indicates that the interaction with the ion of electrons that return with small impact parameter should be reasonably well described by a contact interaction, while those that undergo a glancing collision may hardly interact at all. The two results combined seem to suggest that only those electrons make a significant contribution to NSMI that return with small impact parameter, and for those a contact interaction should afford a fair description. However, the long range of Coulomb interaction restricts the significance of the smallness of the de Broglie wavelength. Hence, one cannot assess the situation with certainty, and we will proceed to investigate the consequences of both scenarios.

Equation (1) specifies a fully ( $3N$ -fold) differential momentum distribution. For comparison with experimental data, nonobserved momentum components have to be integrated over. Here, we will focus on the longitudinal (parallel to the linearly polarized laser field) component  $P_\parallel$  of the ion momentum  $\mathbf{P} = -\sum_{n=1}^N \mathbf{p}_n$  with the two transverse components  $\mathbf{P}_\perp$  integrated over. It is distributed according to

$$F(P_\parallel) = \int \prod_{i=2}^N d^3\mathbf{p}_i \int d^2\mathbf{p}_{1\perp} dp_{1\parallel} \delta\left(P_\parallel + \sum_{i=1}^N p_{i\parallel}\right) F(\mathbf{p}_1, \mathbf{p}_2, \dots, \mathbf{p}_n). \quad (8)$$

For the contact model, the result is [9]

$$F(P_\parallel) = \frac{(2\pi)^{(3N/2)-1/2}}{\sqrt{N}\Gamma((3N-1)/2)} \int dt' R(t') (\Delta E)_+^{(3N/2)-3/2}, \quad (9)$$

where  $\Delta E \equiv E_{\text{ret}}(t) - E_0^{(N)} - 1/(2N)[P_{\parallel} - NA(t + \Delta t)]^2$  and the function  $x_+$  is defined by  $x_+ = \theta(x)x$  with  $\theta(x)$  the unit-step function. For the Coulomb model, the corresponding ion-momentum distribution is

$$F(P_{\parallel}) = \frac{(2\pi)^{(3/2)N-1}}{4\sqrt{N-1}\Gamma((3/2)N-1)} \int dt' R(t') \int dp_{1\parallel} (\Delta E)_+^{(3/2)N-2} \left( \Delta E + \frac{1}{2}(p_{1\parallel} - k)^2 \right)^{-2} \times {}_2F_1 \left( \frac{3}{2}N - 2, 2; \frac{3}{2}N - 1; \frac{\Delta E}{\Delta E + (1/2)(p_{1\parallel} - k)^2} \right), \quad (10)$$

where

$$\Delta E = E_{\text{ret}}(t) - E_0^{(N)} - \frac{1}{2}[p_{1\parallel} + A(t)]^2 - \frac{1}{2}(N-1) \left( A(t + \Delta t) - \frac{1}{N-1}(P_{\parallel} + p_{1\parallel}) \right)^2 \quad (11)$$

and  ${}_2F_1(a, b; c; d)$  denotes the hypergeometric function. In comparison with (9), the integration over  $p_{1\parallel}$  cannot be carried out analytically and is left for numerical computation. The derivation of (10) has been relegated to the appendix.

### 3. Ion-momentum distributions

Below, we will compare the model of  $N$ -electron thermalization mediated by an effective many-body contact potential (cf equations (2) and (3)) and the model of  $(N-1)$ -electron thermalization initiated by the Coulomb interaction (equations (4) and (5)). We expect the following general features to emerge in this comparison. Since the first electron tunnels out right after a maximum of the field, it returns with high velocity, but its drift momentum  $\mathbf{k}$  is low. The Coulomb potential (4) favours as small a momentum and energy transfer as is possible in order that the remaining bound electrons can still be ionized. Hence, the returning electron will continue its path with a velocity that has changed only little and, in consequence, its drift momentum will still be relatively low. Therefore, the peak of the ion-momentum distribution is expected around  $(2N-1)\sqrt{U_P}$  for the Coulomb model in place of  $2N\sqrt{U_P}$  for the contact interaction, where  $U_P$  denotes the ponderomotive potential of the laser field. The energy transfer to the bound electrons is lower than in the case of the contact potential and, therefore, the widths of the two humps of the ion-momentum distribution are narrower. This discussion pertains to the case of small delay  $\Delta t$ . For increasing  $\Delta t$ , the available energy  $E_{\text{ret}}(t) - E_0^{(N)}$  remains the same, but the  $N-1$  initially bound electrons become free at a later time, when the vector potential is smaller. Hence, their drift momenta  $p_{i\parallel}$  will be smaller and, in consequence, the ion's longitudinal momentum  $P_{\parallel}$  will be smaller, too. Therefore, for both models, the peak positions of the two humps will move towards zero momentum with increasing  $\Delta t$ . Also, the vector potential at the release time  $t + \Delta t$  spreads over a larger range when  $\Delta t$  increases, so one expects the widths of the humps to increase.

Indeed, we find the expected features confirmed in figure 2, where we present the calculated longitudinal ion-momentum distributions for quadruple and triple NSMI of Ne, under the two different recollision scenarios considered above, which lead, respectively, to the distributions (9) and (10). The laser intensities are taken as 2 and 1.5 PW cm<sup>-2</sup> for quadruple and triple ionization, respectively, to match the experimental data of Ne in [15, 16]. For both scenarios, the familiar double-hump structure appears in the ion-momentum distributions. The positions of the centre and the widths of the humps exhibit a strong dependence on the time delay  $\Delta t$ . With  $\Delta t$  increasing, the centre positions move towards zero momentum and the widths increase

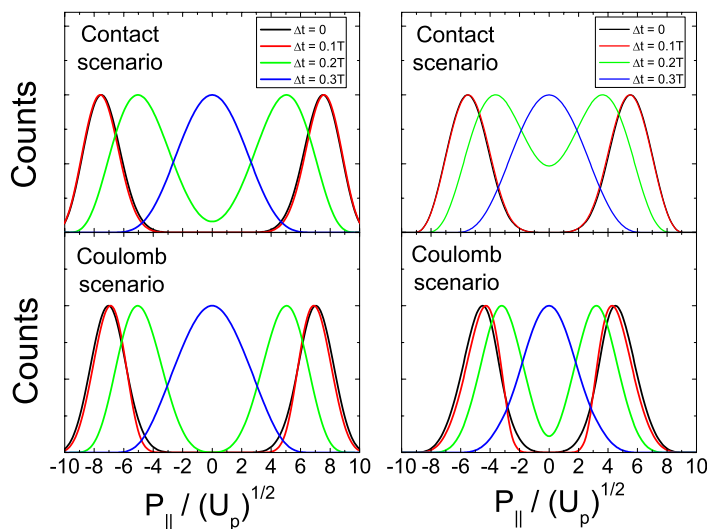


**Figure 2.** Distribution of the longitudinal ion momentum for nonsequential quadruple ionization of Ne at  $2.0 \text{ PW cm}^{-2}$  (left column) and for nonsequential triple ionization of Ne at  $1.5 \text{ PW cm}^{-2}$  (right column), calculated from (9) for the contact scenario (upper panels) and (10) for the Coulomb scenario (lower panels), respectively. The various delay times  $\Delta t$  employed in the calculations are indicated in the upper panels.

until the two humps begin to merge. We notice that as expected the humps resulting from the Coulomb scenario are generally somewhat narrower than those from the contact scenario. In particular, the former produces fewer ions with near zero momentum. We also notice that the differences between the two scenarios decrease with increasing  $N$ .

Formally, the differences can be traced to the presence of the additional integration over  $p_{1\parallel}$  in the Coulomb-model ion-momentum distribution (10). Both the hypergeometric function and its prefactor favour values of  $p_{1\parallel}$  close to the drift momentum  $k$ . This corresponds to the case that the returning electron in the recollision transfers minimal momentum and energy to the bound electrons, continues on its path, and leaves the interaction region with comparatively low drift momentum, which leads, accordingly, to small peak momenta in the ion-momentum distribution.

Next, in figures 3 and 4, we compare the results of the two versions of the thermalization model with the experimental data for quadruple and triple ionization of Ne [15], respectively. The curves in the upper panels are calculated from (9) under the contact scenario, while in the lower panels the curves are calculated from (10) under the Coulomb scenario. The red and the green curves correspond to the thermalization times  $\Delta t = 0$  and  $0.17 T$ , respectively. The black curves represent the data of figure 2 of [15]. The choice of the value  $\Delta t = 0.17 T$  is motivated by the fact that this value has been shown to yield, for the contact scenario, the best agreement with the data [9]. In contrast to the contact scenario, for the Coulomb scenario there is no optimal value of the thermalization time that yields equally good agreement with the data for both triple and quadruple ionization. For example, for quadruple ionization (figure 3), the choice  $\Delta t = 0$  yields very poor agreement with the data while  $\Delta t = 0.17 T$  gives acceptable results for the peak position and the width of the humps, but too low counts near zero momentum. In contrast,

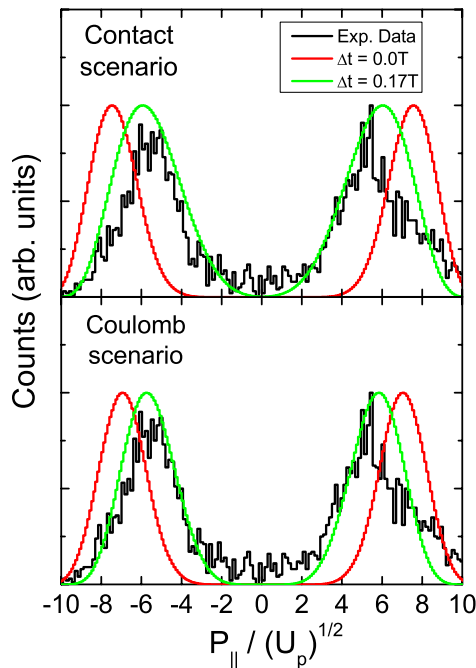


**Figure 3.** Comparison of the ion-momentum distributions of the two model calculations with the experimental data [15] for quadruple ionization of Ne at  $2.0 \text{ PW cm}^{-2}$ . The curves in the upper panel are calculated from (9) for the contact scenario, while in the lower panel they are calculated from (10) for the Coulomb scenario. The red and green curves are for  $\Delta t = 0$  and  $0.17 T$ , respectively. The black curve is from the data of figure 2 of [15].

for triple ionization as shown in figure 4, the best fit of the peak position is afforded by  $\Delta t = 0$ , but as for quadruple ionization the width is narrower than the data, and the distribution around zero momentum vanishes. All in all, if we look for the model that yields the best agreement with the data for one value of the thermalization time and for both triple and quadruple ionizations, we will have to opt for the contact scenario.

Concerning the distribution near zero momentum, one can argue that the data may include a contribution from a partially sequential ionization channel or an excitation-tunnelling channel, both of which give rise to counts at zero momentum and tend to increase the width of the ion-momentum distribution. As we will show below in the calculations for Ar, the excitation-tunnelling mechanism can be well accounted for within the thermalization model. However, the sequential ionization channel is beyond the scope of the model. Nevertheless, their contributions should be negligible for NSMI of Ne at the laser intensities of interest.

In the contact scenario, all  $N$  electrons thermalize, while in the Coulomb scenario the returning electron after transferring some energy to the bound electrons continues on its path, and only the latter  $N - 1$  electrons thermalize. In order to better understand the differences between these two models, we will consider a third scenario, which is a mix of the first two: there is one common contact interaction between all  $N$  electrons, but the returning electron remembers its identity and leaves immediately at the recollision time  $t$ , not participating in the thermalization process. Formally, this means taking the energy conservation condition (5) and

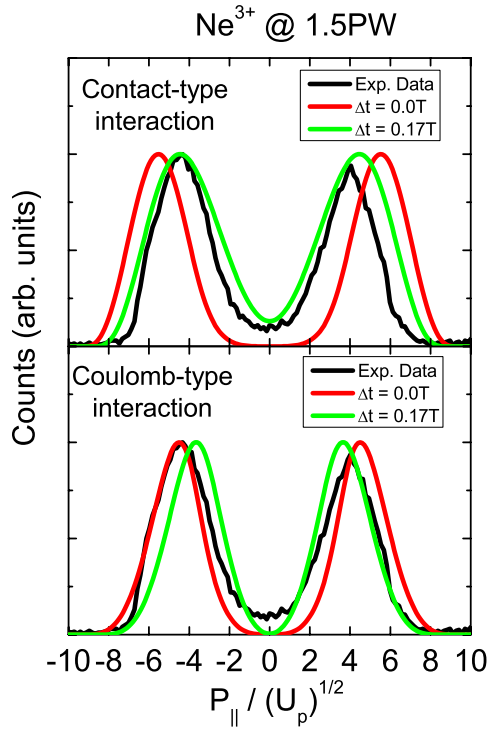


**Figure 4.** Same as figure 3 for triple ionization of Ne at  $1.5 \text{ PW cm}^{-2}$ .

a constant form factor (2) in equation (1). We will refer to this as the  $\text{contact}_{N-1}$  scenario. The longitudinal-ion-momentum distribution corresponding to (10) and (9) is like (9) but with the parameter  $\Delta E$  from equation (11). Comparing this with the  $\text{contact}_N$  scenario will allow us to assess the role of the Coulomb potential in NSMI in the context of our model description.

In figure 5, we compare the results of these three models for triple NSMI of neon at  $1.5 \text{ PW cm}^{-2}$ . The  $\text{contact}_N$  and the  $\text{contact}_{N-1}$  models agree with respect to the centre positions of the double hump, but the latter model causes a significantly narrower width and fewer counts around zero momentum. Comparing the  $\text{contact}_{N-1}$  and the Coulomb scenario reveals the consequences of the Coulomb form factor, all other things being equal. We observe that the Coulomb form factor causes an additional shift of the centre of the humps to lower momentum and an additional decrease of the width. Comparison with the data shown in figure 4 favours the  $\text{contact}_N$  scenario, with the Coulomb scenario faring worst.

Next, we apply our thermalization model to the case of NSMI of argon. As we concluded above for NSMI of neon, the contact model with all  $N$  electrons thermalizing gives the best description. Thus, we only perform the calculations with this scenario according to (9) and compare with the Ar data. Figure 6 exhibits the calculated results. The laser intensities of  $1.2$  and  $1.5 \text{ PW cm}^{-2}$  are chosen to match the experimental conditions of figure 5 of [16]. We find excellent agreement with the data, if the larger delay time  $\Delta t = 0.265 T$  is taken. This suggests that in the case of argon the redistribution of the excess energy between the recolliding electron and the bound electrons requires more time than for neon. The optimal delay of  $\Delta t = 0.265 T$  is very close to a quarter of the field period. At this time, the escape of an excited complex of electrons, be it by tunnelling or over the barrier, is easiest. Hence, one may also conclude that thermalization is fast but the electrons do not leave before the field is near its maximum. We note

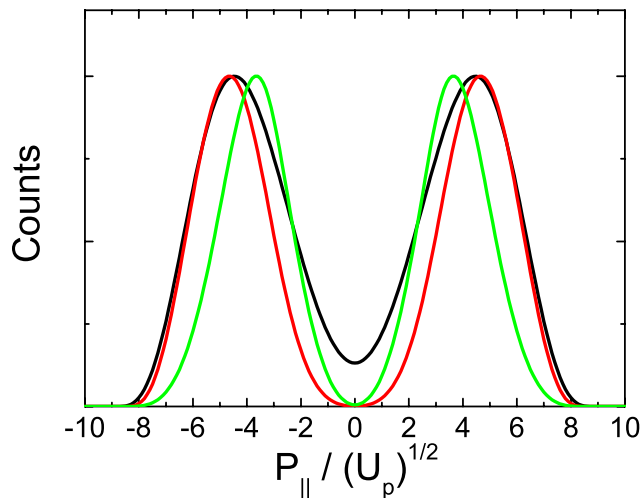


**Figure 5.** Distribution of the longitudinal ion momentum for nonsequential triple ionization of Ne at  $1.5 \text{ PW cm}^{-2}$  calculated from three different thermalization scenarios, i.e. thermalization with all  $N$  electrons (black) and  $N - 1$  electrons (red) under the contact-type interaction, and thermalization of the  $N - 1$  bound electrons under the Coulomb-type interaction (green). The same time delay  $\Delta t = 0.17 T$  is chosen for all calculations.

that, while the contact model does not explicitly contain any specific dynamics, the physical origin of the thermalization time  $\Delta t$  and its value for a specific situation are rooted in the dynamics of the problem. The *same* value of  $\Delta t$  may reflect *different* dynamical mechanisms, such as the actual formation and the subsequent decay of an excited complex [27] or, on the other hand, the time interval during which an excited complex after it has been formed is waiting for optimal conditions for the escape [28]. For the higher laser intensity of  $1.5 \text{ PW cm}^{-2}$ , the calculated momentum distribution for Ar becomes a bit wider than that of the data. This may arise from the fact that the sequential-ionization channels, whose contribution is not included in the model, contribute more significantly with increasing laser intensity.

We could further test the model and possibly infer a tighter limit on the thermalization time. All that is necessary for that purpose is to restrict the time range  $\Delta t_{\text{rec}}$  of the recollision times. The easiest way is simply to decrease the laser intensity. Therefore, we investigate the dependence of the peak position and the width of the ion-momentum distribution as a function of the laser intensity for various time delays  $\Delta t$ . For the contact model, the results are shown in figure 7. We find that the peak position (in units of the square root of the ponderomotive energy) hardly changes for different laser intensities if the time delay  $\Delta t$  is fixed. This can be well understood from the recollision kinematics. The peak position of the ion-momentum distribution is, to a large extent, determined by those collisions through which the bound electrons get free after some time delay and acquire the maximal drift energy from the laser field. Those collision events scale with the square root of the laser intensity for fixed delay. With increasing delay, as soon as the electric field at the time  $t_{\text{ret}} + \Delta t$  becomes significantly different from zero, the drift momentum that the freed electrons acquire from the field decreases and so does the ion momentum. The humps of the ion-momentum distributions become broader with increasing intensity and increasing time delay. The first is due to the increasing volume of the classically allowed phase space, the second is due to the fact that the range of values of the

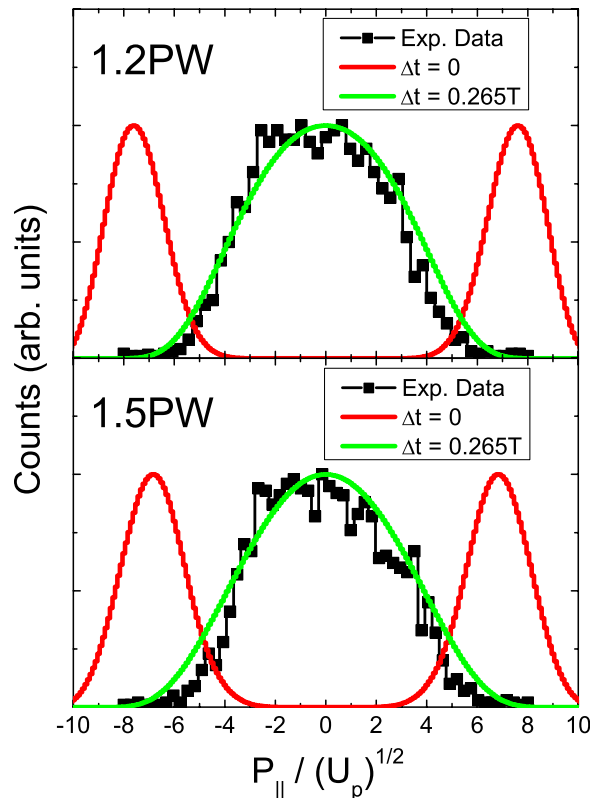


**Figure 6.** Distribution of the longitudinal ion momentum for nonsequential quadruple ionization of Ar at  $1.2 \text{ PW cm}^{-2}$  (upper panel) and  $1.5 \text{ PW cm}^{-2}$  (lower panel). The black curves are from the data of figure 5 of [16]. The red and green curves are calculated from the contact scenario (9), for  $\Delta t = 0$  and  $\Delta t = 0.265 T$ , respectively.

vector potential  $A(t + \Delta t)$  (where  $E_{\text{ret}}(t) > E_0^{(N)}$ ) increases. In other words, the ion-momentum distribution becomes narrower for decreasing intensity. This might allow higher precision for the determination of the thermalization time through a comparison of our theoretical results with experimental low-intensity data. However, the intensity must remain high enough for our classical model to remain applicable.

#### 4. Conclusions

We have investigated the momentum distribution of the multiply charged ions generated by nonsequential  $N$ -fold ionization of atoms within the context of a thermalization model, under different scenarios for the recollision dynamics and the subsequent thermalization process. We have compared two possible interaction potentials by which the recolliding electron shares its energy with the other  $N - 1$  bound electrons. The first is a contact interaction between all  $N$  electrons, which corresponds to a completely statistical distribution of the available energy, governed only by phase space. In the second, the recolliding electron Coulomb interacts with the bound electrons, which thereafter statistically share the imparted energy among each other. Both interactions should be interpreted as *effective* interactions [29]. The contact interaction

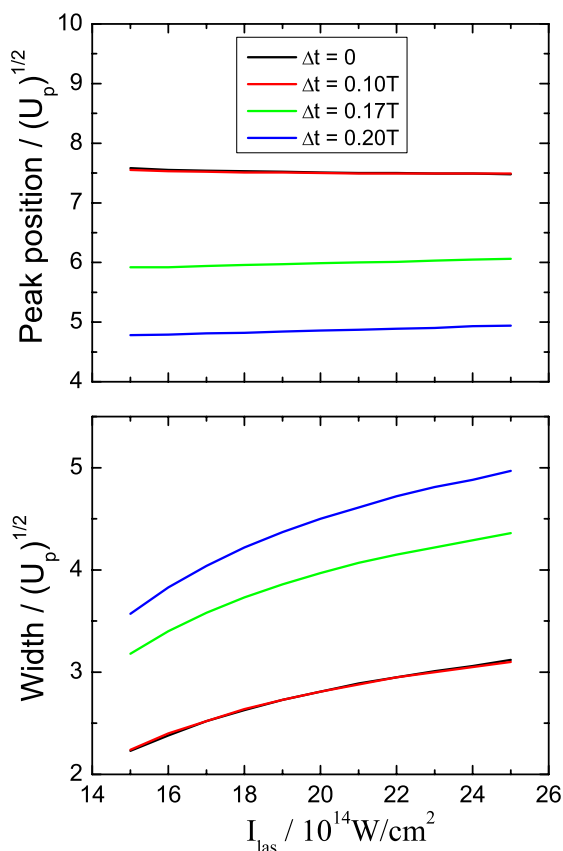


**Figure 7.** The peak position and the width (FWHM) of the humps of the ion-momentum distribution as functions of the laser intensity for various time delays  $\Delta t$  as shown in the upper panel. The calculation is for the contact model and for quadruple ionization of Ne. Note that the results for  $\Delta t = 0$  and  $0.1 T$  are practically identical.

is definitely realized in the low-energy limit when the wavelength of the returning electron after freeing the bound electrons exceeds the ionic diameter. The Coulomb interaction favours glancing collisions where the returning electron changes its momentum as little as possible. In both cases, we assumed that the energy redistribution requires a time  $\Delta t$ , the ‘thermalization time’. The returning electron may leave immediately after the recollision or may participate in the thermalization process and leave after the delay  $\Delta t$ .

The two interaction scenarios yield qualitatively similar ion-momentum distributions. As long as the delay  $\Delta t$  is not too large, the distributions exhibit two pronounced and well separated humps. With increasing delay, the peak positions of the humps move towards zero momentum and with the delay approaching a quarter period of the laser field they merge. For the Coulomb scenario, the ion momenta corresponding to the peak positions and the widths of the humps are somewhat smaller than for the contact scenario. Also for the Coulomb scenario, there are fewer ions with momenta near zero. It does not make much difference whether or not the returning electron participates in the thermalization.

The calculated ion-momentum distributions have been compared with the available data of triple and quadruple nonsequential ionization of neon. We were able to obtain reasonably good

fits for both models. However, for the Coulomb model we had to assume different values of the thermalization time for triple and for quadruple ionization. Only the contact model provided uniformly good agreement with all available neon data with just one universal value, namely  $\Delta t = 0.17 T$ . On these grounds, we favour the contact model and employed it for argon as well. Indeed, we obtained excellent agreement with the quadruple-ionization data in argon for  $\Delta t = 0.265 T$ .

In our statistical thermalization model, all of the dynamics of the physical system between the time of recollision and the time when the electrons leave the ion are hidden in two items: the choice of the effective interaction and the value of the delay  $\Delta t$ , which is the sum of the thermalization time and a possible additional ‘dwell time’. The returning electron may form an excited complex with  $N - 1$  bound electrons [27]. Its subsequent decay may be affected by the field, as it is trivially the case if one considers the fact that the escape threshold is lowered by an applied field [28]. Both of these effects are subsumed by the concept of the delay  $\Delta t$  and parametrized by the value of this delay. Hence, the same value of  $\Delta t$  may reflect very different dynamics which, however, within our model will be indistinguishable. For NSDI of neon and argon, the cross-sections for impact ionization and for excitation-tunnelling have been estimated [19]. If the latter is dominant, as it is for NSDI of argon, we expect that the total delay  $\Delta t$  will be close to  $T/4$ , given that the first electron returns near a zero crossing of the field. For NSMI these cross-sections are not known. For NS3I and NS4I of argon, we found  $\Delta T = 0.265T \approx T/4$ . We may conclude from this result that for NS3I and NS4I of argon, like for NSDI, the excitation-tunnelling cross-section dominates the one for impact ionization. In contrast, if the prevalent mechanism is electron-impact ionization, as appears to be the case for neon, one expects the electrons to leave within a shorter time interval. This is compatible with the estimated upper bound of  $\Delta t = 0.17 T$  for the thermalization time in neon.

We also investigated the dependence of the peak positions and widths of the ion-momentum distribution as a function of the laser intensity for various time delays. We found, for the contact model, that the peak width is very sensitive to both the laser intensity and the time delay, especially for low intensity and not too small delay. Because of this rapid dependence, this parameter region will allow for a particularly meaningful comparison between the model and reality.

More detailed COLTRIMS data, such as electron–electron momentum correlations, will hopefully become available. Such data may lend further support to one or other version of the thermalization model and test its limits.

## Acknowledgments

WB acknowledges fruitful discussions with S P Goreslavski, S V Popruzhenko, and D F Zaretsky. XL acknowledges support from the NNSF of China (no 10674153) and CFMF from the UK Engineering and Physical Sciences Research Council (grant no EP/D07309X/1).

## Appendix. Evaluation of the Coulomb-scenario ion-momentum distribution

The distribution of the ion momentum  $P_{\parallel}$  parallel to the laser field is obtained by integrating over all electron momenta subject to the condition that  $P_{\parallel} = -\sum_{i=1}^N p_{i\parallel}$ . For the second model

specified by (4) and (5), this is

$$F(P_{\parallel}) = \int \prod_{i=2}^N d^3 \mathbf{p}_i \int d^2 \mathbf{p}_{1\perp} dp_{1\parallel} \int dt' R(t') \delta \left( P_{\parallel} + \sum_{i=1}^N p_{i\parallel} \right) \frac{1}{[\mathbf{p}_{1\perp}^2 + (p_{1\parallel} - k)^2]^2} \\ \times \delta \left( E_0^{(N)} - E_{\text{ret}}(t) + \frac{1}{2} [\mathbf{p}_1 + \mathbf{A}(t)]^2 + \frac{1}{2} \sum_{i=2}^N [\mathbf{p}_i + \mathbf{A}(t + \Delta t)]^2 \right). \quad (\text{A.1})$$

The multiple integrals in the above equation may be evaluated largely analytically. To this end, we replace the two delta functions by their Fourier representations and exponentialize the form factor via

$$(A - i\epsilon)^{-\beta} = \frac{e^{i\pi\beta/2}}{\Gamma(\beta)} \int_0^{\infty} dx x^{\beta-1} e^{-ixA}, \quad (\beta \neq 0, -1, -2, \dots). \quad (\text{A.2})$$

This yields

$$F(P_{\parallel}) = \int \prod_{i=2}^N d^3 \mathbf{p}_i \int d^2 \mathbf{p}_{1\perp} dp_{1\parallel} \int dt' R(t') \int_{-\infty}^{\infty} \frac{dx}{2\pi} e^{-ix(P_{\parallel} + \sum p_{i\parallel})} \\ \times \int_0^{\infty} \left( -\frac{ydy}{4} \right) e^{-iy/2(\mathbf{p}_{1\perp}^2 + (p_{1\parallel} - k)^2)} \int_{-\infty}^{\infty} \frac{d\lambda}{2\pi} e^{-i\lambda\eta(\mathbf{p}_i, t, \Delta t)}, \quad (\text{A.3})$$

with

$$\eta(\mathbf{p}_i, t, \Delta t) = E_0^{(N)} - E_{\text{ret}}(t) + \frac{1}{2} \mathbf{p}_{1\perp}^2 + \frac{1}{2} [p_{1\parallel} + A(t)]^2 + \frac{1}{2} \sum_{i=2}^N [\mathbf{p}_{i\perp}^2 + (p_{i\parallel} + A(t + \Delta t))^2]. \quad (\text{A.4})$$

Next, we do the integrals over  $\mathbf{p}_i (i = 2, \dots, N)$  and  $\mathbf{p}_{1\perp}$  by Gaussian quadrature, with the result

$$F(P_{\parallel}) = \int dp_{1\parallel} \int dt' R(t') \int_{-\infty}^{\infty} \frac{dx d\lambda}{(2\pi)^2} e^{-ix(P_{\parallel} + p_{1\parallel})} \int_0^{\infty} \left( -\frac{ydy}{4} \right) \left( \frac{2\pi}{i\lambda + \epsilon} \right)^{(3/2)(N-1)} \\ \times \frac{2\pi}{i(\lambda + y) + \epsilon} e^{-i(y/2)(p_{1\parallel} - k)^2} \exp \left[ -i\lambda\zeta_1 \left( E_0^{(N)}, p_{1\parallel}, t \right) \right] \exp \left[ i\zeta_2(x, N, \lambda, t + \Delta t) \right], \quad (\text{A.5})$$

where

$$\zeta_1 \left( E_0^{(N)}, p_{1\parallel}, t \right) = E_0^{(N)} - E_{\text{ret}}(t) + \frac{1}{2} [p_{1\parallel} + A(t)]^2, \quad (\text{A.6})$$

and

$$\zeta_2(x, N, \lambda, t + \Delta t) = (N - 1) \left[ \frac{x^2}{2\lambda} + xA(t + \Delta t) \right]. \quad (\text{A.7})$$

The integration over  $x$  is another Gaussian quadrature and yields

$$F(P_{\parallel}) = - \int dp_{1\parallel} \int dt' R(t') \int_{-\infty}^{\infty} d\lambda \int_0^{\infty} \frac{ydy}{4\sqrt{N-1}} \left( \frac{2\pi}{i\lambda + \epsilon} \right)^{(3/2)N-2} \\ \times \frac{1}{i(\lambda + y) + \epsilon} e^{-i(y/2)(p_{1\parallel} - k)^2} e^{i\lambda\Delta E}, \quad (\text{A.8})$$

where

$$\Delta E = E_{\text{ret}}(t) - E_0^{(N)} - \frac{1}{2} [p_{1\parallel} + A(t)]^2 - \frac{1}{2} (N - 1) \left( A(t + \Delta t) - \frac{1}{N-1} (P_{\parallel} + p_{1\parallel}) \right)^2. \quad (\text{A.9})$$

The integral over  $\lambda$  yields a confluent hypergeometric function via the formula

$$\int_{-\infty}^{\infty} \frac{d\lambda}{(i\lambda + \epsilon)^n (i(\lambda + y) + \epsilon)} e^{i\lambda A} = 2\pi \frac{A_+^n}{\Gamma(n+1)} e^{-iAy} {}_1F_1(n, n+1; iyA), \quad (\text{A.10})$$

where  $x_+^n = x^n \theta(x)$  with  $\theta(x)$  the unit step function. This leads to the ion-momentum distribution

$$F(P_{\parallel}) = (2\pi)^{(3/2)N-1} \int dt' R(t') \int dp_{\parallel} \int \frac{y dy}{4\sqrt{N-1}} e^{-i(y/2)(p_{\parallel}-k)^2} \frac{(\Delta E)_+^{(3/2)N-2}}{\Gamma(\frac{3}{2}N-1)} \times {}_1F_1\left(\frac{3}{2}N-2, \frac{3}{2}N-1; iy\Delta E\right). \quad (\text{A.11})$$

The remaining integration over  $y$  can be carried out with the help of the integral

$$\int_0^{\infty} dy e^{-sy} y^{b-1} {}_1F_1(a, c; ky) = \Gamma(b) s^{-b} {}_2F_1(a, b; c; k/s), \quad (\text{A.12})$$

and yields expression (10), which is given in the main body of the paper.

## References

- [1] L'Huillier A, Lompré L A, Mainfray G and Manus C 1983 *Phys. Rev. A* **27** 2503
- [2] Fittinghoff D N, Bolton P R, Chang B and Kulander K C 1992 *Phys. Rev. Lett.* **69** 1992  
Larochelle S, Talebpour A and Chin S L 2003 *J. Phys. B: At. Mol. Opt. Phys.* **31** 1201
- [3] Becker A, Dörner R and Moshhammer R 2005 *J. Phys. B: At. Mol. Opt. Phys.* **38** S753
- [4] Corkum P B 1993 *Phys. Rev. Lett.* **71** 1994
- [5] Scrinzi A, Ivanov M Yu, Kienberger R and Villeneuve D 2006 *J. Phys. B: At. Mol. Opt. Phys.* **39** R1  
Corkum P B and Krausz F 2007 *Nat. Phys.* **3** 381
- [6] Niikura H *et al* 2002 *Nature* **417** 917  
Niikura H *et al* 2003 *Nature* **421** 826
- [7] Parker J S, Doherty B J S, Meharg K J and Taylor K T 2003 *J. Phys. B: At. Mol. Opt. Phys.* **36** L393  
Taylor K T, Parker J S, Meharg K J and Dundas D 2003 *Eur. Phys. J. D* **26** 67
- [8] Ruiz C, Plaja L, Roso L and Becker A 2006 *Phys. Rev. Lett.* **96** 053001
- [9] Liu X, Figueira de Morisson Faria C, Becker W and Corkum P B 2006 *J. Phys. B: At. Mol. Opt. Phys.* **39** L305
- [10] Figueira de Morisson Faria C and Liu X 2007 *J. Mod. Opt.* **54** 1107
- [11] Russek A 1963 *Phys. Rev.* **132** 246
- [12] Hagedorn R 1965 *Nuovo Cimento Suppl.* **3** 147
- [13] Forst W 1973 *Theory of Unimolecular Reactions* (New York: Academic)  
Robinson P J and Holbrook K A 1972 *Unimolecular Reactions* (New York: Wiley)
- [14] Panfili R, Haan S L and Eberly J H 2002 *Phys. Rev. Lett.* **89** 113001
- [15] Rudenko A, Zrost K, Feuerstein B, de Jesus V L B, Schröter C D, Moshhammer R and Ullrich J 2004 *Phys. Rev. Lett.* **93** 253001
- [16] Zrost K, Rudenko A, Ergler Th, Feuerstein B, de Jesus V L B, Schröter C D, Moshhammer R and Ullrich J 2006 *J. Phys. B: At. Mol. Opt. Phys.* **39** S371
- [17] Moshhammer R *et al* 2000 *Phys. Rev. Lett.* **84** 447
- [18] Weber Th *et al* 2000 *J. Phys. B: At. Mol. Opt. Phys.* **33** L127
- [19] de Jesus V L B, Feuerstein B, Zrost K, Fischer D, Rudenko A, Afaneh F, Schröter C D, Moshhammer R and Ullrich J 2004 *J. Phys. B: At. Mol. Opt. Phys.* **37** L161
- [20] Staudte A *et al* 2007 *Phys. Rev. Lett.* **99** at press  
Rudenko A *et al* 2007 *Phys. Rev. Lett.* **99** at press

- [21] Landau L D and Lifshitz E M 1977 *Quantum Mechanics (Nonrelativistic Theory)* (Oxford: Pergamon)
- [22] Figueira de Morisson Faria C, Liu X, Becker W and Schomerus H 2004 *Phys. Rev. A* **69** 021402
- [23] Figueira de Morisson Faria C, Schomerus H, Liu X and Becker W 2004 *Phys. Rev. A* **69** 043405
- [24] Corkum P B, Burnett N H and Brunel F 1989 *Phys. Rev. Lett.* **62** 1259
- [25] Delone N B and Krainov V P 1991 *J. Opt. Soc. Am. B* **8** 1207
- [26] Gottlieb B, Lohr A, Becker W and Kleber M 1996 *Phys. Rev. A* **54** R1022
- [27] Sacha K and Eckhardt B 2001 *Phys. Rev. A* **64** 053401  
Sacha K and Eckhardt B 2003 *J. Phys. B: At. Mol. Opt. Phys.* **36** 3923
- [28] Eremina E *et al* 2003 *J. Phys. B: At. Mol. Opt. Phys.* **36** 3269
- [29] Figueira de Morisson Faria C, Liu X and Becker W 2007 *Progress in Ultrafast Intense Laser Science II (Springer Series in Chemical Physics)* ed K Yamanouchi, S L Chin, P Agostini and G Ferrante (Berlin: Springer) p 65